Soil Dynamics and Earthquake Engineering xxx (xxxx) xxx–xxx

Contents lists available at ScienceDirect

Soil Dynamics and Earthquake Engineering

journal homepage: www.elsevier.com/locate/soildyn

Applicability of sliding block analyses for lateral spreading problems

Andrew J. Makdisi[a], Steven L. Kramer[b]

[a] Hart Crowser Inc., Seattle, WA, 98121, USA
[b] Department of Civil and Environmental Engineering, University of Washington, Seattle, WA, 98195, USA

ABSTRACT

Liquefaction-induced lateral spreading deformations can significantly affect the seismic performance of bridge pile foundations, shallow foundation systems, and critical underground infrastructure. Current simplified approaches for predicting lateral spreading displacements largely neglect complex ground motion, material, hydraulic, and topographic factors that influence them. Newmark sliding block analyses based on back-calculated liquefied shear strengths have also been proposed for prediction of lateral spreading displacements. However, certain assumptions of the sliding block method (e.g., deformations along a discrete failure surface, rigid perfectly-plastic soil behavior, and constant shearing resistance) are inconsistent with the actual mechanics of lateral spreading. In this study, the applicability of sliding block analyses to lateral spreading displacement prediction was assessed in terms of biases in displacement predictions and uncertainty in both predicted displacements and the back-calculated shear strengths upon which they are based. A probabilistic analysis using the sliding block-based framework indicated that significant uncertainties, primarily related to characterization of the liquefied soil and record-to-record ground motion variability, resulted in extremely low precision in both predicted displacements and back-calculated shear strengths. Furthermore, a comparative analysis between sliding block, empirical, strain potential-based, and numerical methods showed that the sliding block model generally produced significantly lower displacement predictions than the other approaches. These sources of uncertainty and biases in the sliding block framework have a strong impact on the evaluation of lateral spreading in both traditional and performance-based frameworks.

1. Introduction

Liquefaction-induced lateral spreading has caused significant damage to bridges, embankments, wharves, pipelines and other important elements of infrastructure in many past earthquakes. Lateral spreading occurs when liquefaction is triggered in soils beneath sloping ground surfaces or under flat ground adjacent to slopes such as riverbanks, shorelines, and embankments. The ground deformations associated with lateral spreading are often irregular in amplitude and location, and can impose significant deformation demands on structures supported on, or on foundations extending through, liquefiable soil deposits.

Geotechnical engineers are often called on to estimate permanent deformations caused by lateral spreading, either for the resilient design of structures it may affect, or for the design of soil improvement measures that may be used to mitigate the lateral spreading hazard. Because the mechanics of lateral spreading are so complex, lateral spreading deformations have historically been estimated by empirical methods based on correlation to case history observations. More recently, methods based on both simple and more complex dynamic analyses have been used for estimation of lateral spreading displacements. The simple methods take the form of sliding block analyses, which have been proposed, most recently [18], for use with sliding resistances tied to the residual strength of the liquefied soil. This paper examines the assumptions inherent in sliding block analyses and the various steps involved in applying them to the lateral spreading problem, and assesses the uncertainty inherent in sliding block estimates of lateral spreading deformations. Finally, the sliding block method is compared against three other lateral spreading frameworks to evaluate its ability to predict lateral spreading displacements across a wide range of site and earthquake source conditions.

2. Background

Lateral spreading is a form of slope instability that involves both transient inertial loading and simultaneous changes in soil stiffness and strength. It is influenced by both the mechanical and hydraulic behavior of the soil and porewater, and can be sensitive to site conditions that are difficult to characterize in advance of an earthquake. This situation leads to significant challenges in estimation of lateral spreading deformations, and a number of different approaches to meeting those

E-mail address: ajmakdisi@gmail.com (A.J. Makdisi).

https://doi.org/10.1016/j.soildyn.2018.04.040
Received 30 September 2017; Received in revised form 29 March 2018; Accepted 25 April 2018

challenges have been proposed.

2.1. Seismic Slope Stability

Evaluation of the seismic stability of slopes begins with evaluation of static stability, which is usually performed using limit equilibrium analyses. Limit equilibrium analyses (LEA) typically consider the driving stresses acting on a potential failure surface, and compare them to the available shear strength along the surface via the factor of safety. The factor of safety, *FS*, is taken as an index of the static stability of the slope – $FS < 1.0$ implies "failure," but does not provide any indication of the consequences of that failure. Limit equilibrium analyses imply rigid-perfectly plastic material behavior on and above the failure surface.

The earliest, and still frequently used, form of seismic slope stability analysis is pseudo-static analysis. Pseudo-static analysis is an extension of the LEA, whereby seismic loading is represented by a horizontal force that is added to the driving forces above the failure surface, which generally acts to destabilize the slope relative to the static condition. The representation of seismic loading in this manner is a significant over-simplification, as the inertial forces induced by earthquake shaking are not constant and act in both the downslope and upslope directions. Furthermore, the pseudo-static factor of safety still provides no indication of the potential consequences of failure. The pseudo-static approach can be used to compute the acceleration amplitude at which the pseudo-static factor of safety is equal to 1.0, which is referred to as the yield acceleration, a_y, of the slope. Yield accelerations can be computed for sliding in both the upslope and downslope directions; a_y for upslope sliding is usually so much higher than that for downslope sliding that one-way sliding in the downslope direction is generally assumed in such analyses.

Recognizing that relative displacements between the materials above and below a failure surface would occur (under the rigid-perfectly plastic assumptions of LEA) when the yield acceleration was exceeded, Newmark [16] proposed a method of deformation analysis based on a sliding block moving relative to a frictional surface. The conventional sliding block analysis assumes that a rigid failure mass will begin to slide with constant shearing resistance on a discrete failure surface when it is subjected to a base acceleration greater than the yield acceleration, and will continue to do so until the acceleration drops below a_y long enough for the slope to decelerate to zero relative velocity. The relative acceleration can be double-integrated over time to compute the relative displacement of the failure mass. Fig. 1 shows the time history of displacement of a seismically unstable slope and the shear stress-displacement history computed from a one-way sliding block analysis, which is the approach used to develop the OJ08 sliding block procedure. The shear stress-displacement history shows the rigid-perfectly plastic behavior of the interface – the unstable soil does not move until the strength of the interface is reached, so it is either not moving or is moving with a constant shearing resistance. The displacement increases (and only increases) in a series of incremental steps when the shear strength is reached.

2.2. Liquefaction and lateral spreading

Fig. 2 shows a time history of shear strain and the stress-strain behavior from a cyclic simple shear test performed on a sand sample subjected to transient loading under an initial, static shear stress, which is representative of conditions that exist in the field during lateral spreading. The stress-strain behavior shows a relatively high initial stiffness, extreme softening as pore pressures develop, and evidence of dilation-induced stiffening due to phase transformation behavior – a complex behavior that is clearly very different from the simple rigid-perfectly plastic behavior implied by the assumptions of the sliding block model. The shear strain time history shows strain developing in a series of both positive and negative increments, but with an overall net positive permanent strain of nearly 15% due to the initial static shear stress applied to the specimen. The available shearing resistance is never constant.

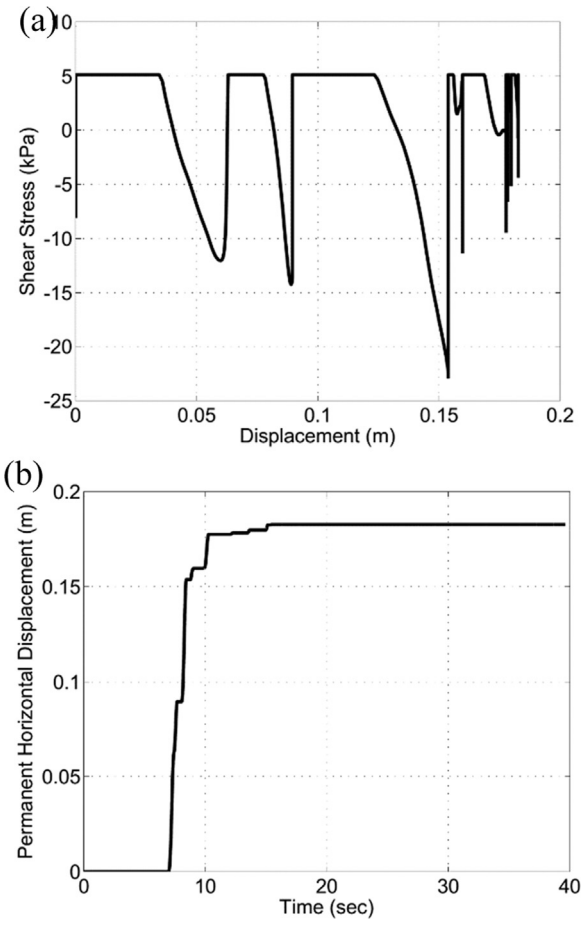

Fig. 1. Results of typical sliding block analysis: (a) shear stress-displacement behavior on interface with 5 kPa strength and (b) sliding displacement history.

In the field, the deformations produced by lateral spreading are typically distributed over the thickness of a liquefiable layer. The liquefiable layer can be visualized as a stack of sublayers each responding to the loading imposed upon them in the complex manner of the test specimen shown in Fig. 2. The total displacement of the layer would be equal to the sum of the products of the strain and thickness of each sublayer.

2.3. Lateral spreading case histories

Most lateral spreading models are empirically-based. Some are direct empirical models obtained by regression against lateral spreading case histories, some are based on laboratory data and field case histories, and some use case histories to validate numerical analyses. Sliding block lateral spreading models fall into the latter category, so an examination of their applicability requires examination of the case history data used in their development. A case history database developed by Olson and Johnson [18] to back-calculate shear strength ratios used in their sliding block model, can be compared to the previously established database used by Youd et al. [25] to develop their direct empirical model. While the OJ08 database is considerably smaller (39 case histories) than the Youd database (484 cases), it samples from a more even distribution of sites and events. Over 75% of the case histories in the Youd et al. database come from only two events (1964 Niigata and 1983 Nihonkai-Chubu), resulting in a source-site distance distribution that is skewed heavily towards these two events

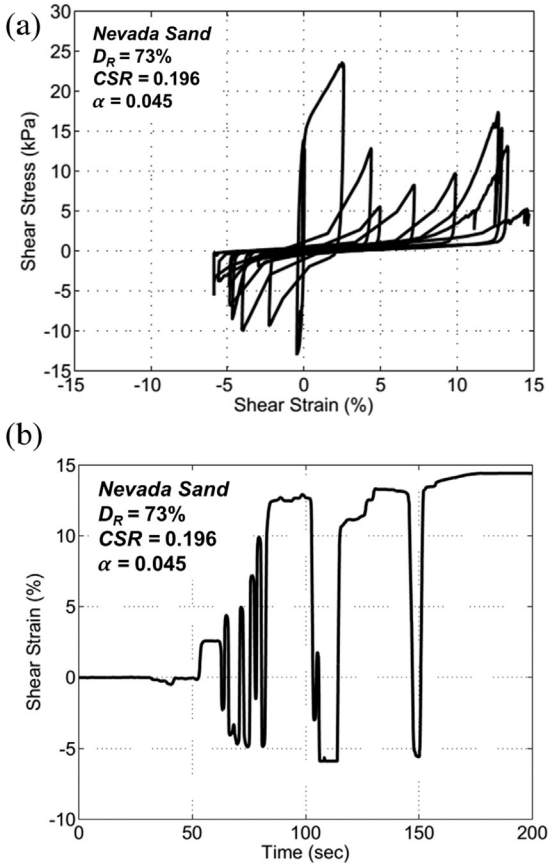

Fig. 2. (a) Shear stress-strain behavior and (b) shear strain history from cyclic simple shear test on Nevada Sand (D_R = 73%) subjected to transient loading.

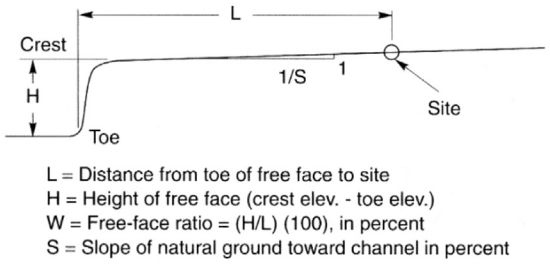

Fig. 3. Notation for geometries of ground-slope and free-face sites (after [1]).

(21 and 27 km, respectively). The OJ08 database contains a comparatively even distribution of source-site distances about its median of about 9 km. The two databases also differ in the types of site topographies contained in each. Nearly 80% of the cases surveyed by Youd et al. involved sites with ground slope inclinations less than 1%. On the other hand, nearly 75% of cases in the OJ08 database correspond to free-face sites Fig. 3. For those case histories, free-face ratios averaged about 23%. Bartlett and Youd [1] indicated that ground deformations tend to be influenced by effects other than lateral spreading at free-face ratios greater than 20%. Thus, the displacements in a significant fraction (over 60%) of the cases in the OJ08 database may be influenced by mechanisms other than lateral spreading.

A particularly well-documented case history of lateral spreading was that observed at Moss Landing in the 1989 Loma Prieta earthquake [4], where it caused damage to roadways and to the Moss Landing Marine Laboratory. Fig. 4 shows the soil profile at one of the lateral spreading sites along with ground displacements measured with an inclinometer at a casing installed before the earthquake. The lateral displacements were associated with a medium dense sand layer that

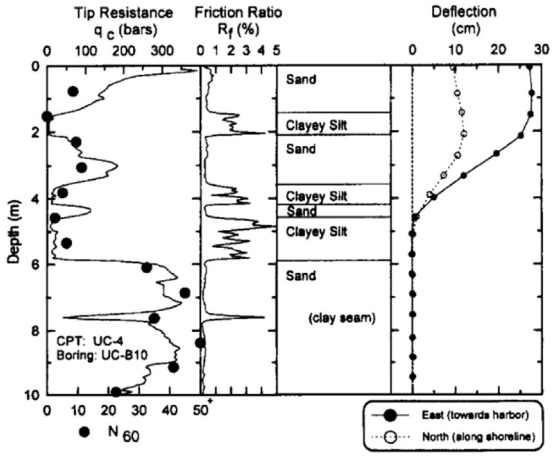

Fig. 4. Subsurface conditions and measured lateral displacement profile from Moss Landing lateral spread case history [4].

extended from about 2.0–3.6 m depth. Correcting for overburden pressure, the median $(N_1)_{60}$ value of that layer was 20 blows/ft. The displacements can be seen to be distributed relatively evenly over the thickness of the sand layer rather than accumulating on a very thin, discrete failure surface.

Another lateral spreading case history with a relative plethora of data was the Wildlife liquefaction array in Southern California, located at the southern terminus of the San Andreas Fault. During the 1987 Superstition Hills earthquake, an array of ground motion recording equipment and pore pressure transducers captured key data when a 3 m-thick layer of loose, saturated sand liquefied at the site, resulting in moderate displacements of about 20 cm towards the Alamo River [3].

2.4. Sliding block analyses of lateral spreading displacements

Castro [7] was the first to suggest the potential applicability of the sliding block method in an analysis of the Heber Road lateral spread from the 1979 Imperial Valley earthquake. Baziar et al. [2] also suggested the use of sliding block analyses for predicting lateral spreading displacements, although emphasizing that characterizing the post-liquefaction residual shear strength could be problematic.

More recently, Olson and Johnson [18] presented a sliding block procedure for prediction of lateral spreading displacement. The procedure involves the performance of sliding block analyses with yield accelerations computed using residual strengths assigned to liquefied layers. The procedure was developed by back-calculating liquefied shear strengths from 39 lateral spread case histories in two stages. First, sliding block analyses were used to estimate the yield acceleration of each lateral spread. A suite of 20 acceleration time histories was compiled for each case history, based on the magnitude, rupture mechanism and site conditions associated with that case history. All of the motions were then scaled to the observed or estimated *PGA* at the site. The motions were then used as inputs to a series of one-way sliding block analyses for a range of yield accelerations. The displacement observed in the field was then used to determine the median yield acceleration for the case history (Fig. 5a). Both the observed displacement and median yield acceleration were treated as known, deterministic quantities.

In the second stage, a series of pseudo-static slope stability analyses were used to compute the liquefied shear strength ratio (ratio of shear strength of liquefied soil to initial vertical effective stress) that corresponded to the median yield acceleration computed in the first stage. Using the available site data for each case history, a soil profile of the lateral spread was generated for limit equilibrium slope stability analysis. Then, a series of pseudo-static analyses were performed using search functions to locate the critical failure surface, the liquefied

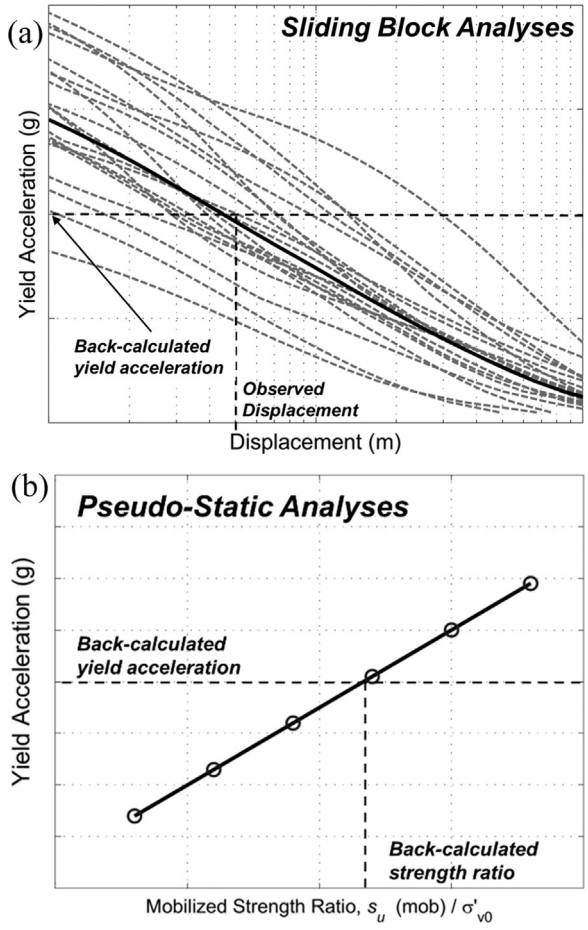

Fig. 5. Schematic illustration of Olson and Johnson [18] framework for back-calculation of MSR from observed displacement.

strength ratio of the liquefiable material was varied to establish a relationship between yield acceleration and liquefied strength ratio (Fig. 5b). The liquefied strength ratio determined in this manner was treated as a known, deterministic quantity.

When the back-calculated liquefied strength ratios ($S_{u,liq}/\sigma'_{vo}$) for the 39 case histories were plotted against their in situ penetration resistances $(N_1)_{60}$ and q_{c1}, Olson and Johnson [18] concluded that the data coincided with the strength ratios back-calculated from liquefaction flow failures by Olson and Stark [17] (Fig. 6). It was also proposed that the same relationship used to estimate mobilized strength ratios from CPT and SPT penetration resistances for flow failures could be used to compute yield accelerations used in sliding block predictions of lateral spreading displacements.

Despite the relative ease of applicability of a sliding block procedure for evaluating lateral spreading displacements, a number of components of the OJ08 sliding block framework have provoked discussion. Moss and Hollenback [15] discussed the uncertainties involved in characterizing SPT and CPT values for the OJ08 case histories. Specifically, they noted that 10 of the 39 cases featured only one (or in two cases, neither) of the two test methods; the authors instead relied on published correlations to convert between Swedish Cone (SWS), SPT, and CPT values. The discussers indicated that using such correlations introduced coefficients of variation (C.O.V.) of approximately 40–120% to the penetration resistance estimate. Park and Kutter [19] analyzed the uncertainties in the correlation equations between penetration resistances and mobilized strength ratio [17] used by OJ08, and found that the coefficient of correlation (R^2) was about 0.4 for the lateral spread dataset. This low R^2 value suggested that there is considerable uncertainty in the relationship between the in situ penetration

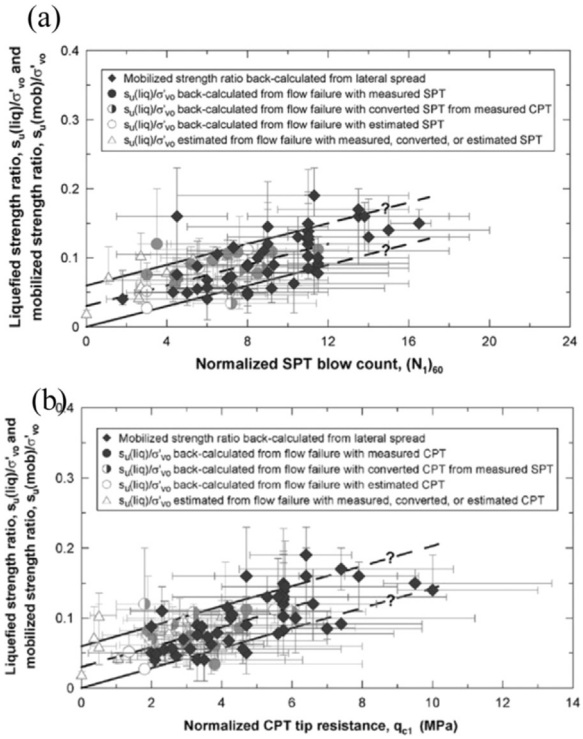

Fig. 6. Relationship between penetration resistance and both liquefied shear and mobilized shear strength ratios, for (a) SPT and (b) CPT data [18].

resistances and mobilized strength ratios estimated by Olson and Johnson [18]. Park and Kutter [19] also noted the strong sensitivity of computed displacement to mobilized strength ratio and pointed out the need to examine computed displacements based on both the upper and lower bounds of the Olson and Stark [17] relationship.

2.5. Issues in the application of sliding block analyses to lateral spreading

The preceding sections have described sliding block analyses, liquefaction and lateral spreading, and an available procedure for estimation of lateral spreading displacements using sliding block analyses. They also pointed out a number of inconsistencies with the actual mechanics of lateral spreading that must be considered when evaluating the applicability of sliding block analyses to lateral spreading problems. They have also reviewed uncertainties pointed out by other in various correlations used in the development of the OJ08 sliding block procedure

Sliding block models assume that deformations are concentrated along a single, discrete sliding surface, and only accumulate displacements when the shear strength along the sliding surface, which is assumed constant, is exceeded. On the other hand, lateral spreading deformations are generally distributed throughout the thickness of the liquefiable material, and can develop due to plastic deformations at shear stresses lower than the shear strength of the soil, which varies significantly over time. Additionally, sliding block models can be performed with two-way sliding either allowed or inhibited. While most slope stability problems do not require a two-way sliding analysis, the flat slopes upon which lateral spreading frequently occurs leads to a relatively low upslope yield acceleration and allows development of incremental displacements in both the upslope and downslope directions.

There are also a number of issues involved in developing a practical and useful sliding block model for accurate, unbiased prediction of lateral spreading displacements over the range of conditions that geotechnical engineers are typically concerned with.

Chief among these issues is the distribution of data used to build the

empirical model. Current lateral spreading databases are not large, and some are dominated by a small number of different earthquakes, soil types, and soil stratigraphy. Additional consideration should be given to how the loading for a given case history is characterized. Ground motion recordings are almost never available at lateral spreading sites, and thus loading must be estimated using ground motion intensity measures, indirect measures of loading (e.g., magnitude and distance), or time histories with similar characteristics to those expected to have occurred at the site. Because lateral spreading displacements can be highly sensitive to the characteristics of the input ground motion, such procedures involve significant uncertainty. If ground motion time histories are used to characterize loading, the method used to select them will play a critical role in the suitability of the sliding block application. Olson and Johnson [18] related sliding block displacements to yield accelerations using suites of ground motions scaled to *PGA* – while this ensures consistency of high-frequency components, lateral spreading deformations occur at soft sites in extremely soft deposits of liquefied soil, and respond more strongly to low-frequency ground motion components.

There is also significant uncertainty in the characterization of a lateral spreading site. Difficulties and complications exist in assigning a single penetration resistance [23] – Olson and Johnson [18] used average penetration resistance over relatively large thicknesses, but lateral spreading deformations are likely to be associated with the looser portions of a layer of liquefiable soil. There is also the issue of characterizing the observed displacements in a lateral spread, which often involves complex distributions of deformations occurring in different directions, via a single estimated value. Finally, current procedures require the slope geometry to be idealized as either a free face or a ground slope, while actual slope topographies may contain elements of both geometries, or may not fit well into either idealized category. All of these issues, those associated with the sliding block model itself and those associated with its application to lateral spreading problems, suggest that lateral spreading displacements computed from sliding block analyses should be considered to be uncertain. In an effort to quantify the level of uncertainty in these computed displacements, a probabilistic analysis of the sliding block procedure was undertaken.

3. Probabilistic evaluation of sliding block-based method

The sliding block procedure uses a mobilized strength ratio computed from a back-calculated yield acceleration to predict lateral spreading displacements. To evaluate the uncertainty in lateral spreading displacement predictions, it is necessary to evaluate the uncertainty in both the back-calculated yield accelerations and back-calculated liquefied strength ratios.

In this section, a probabilistic version of the OJ08 back-analysis procedure is illustrated for a well-known case history analyzed by Olson and Johnson [18]. The goal was to produce estimates of the distributions of yield acceleration and liquefied shear strength, rather than as discrete, deterministic quantities. The case history analyzed is the Monterey Bay Aquarium Research Facility (MBARI 3) in Moss Landing where 25 cm of permanent ground surface displacement (Fig. 4) was observed in the 1989 Loma Prieta earthquake [4]. This case was selected due to its well-documented nature; ground movements and subsurface conditions were well investigated and documented, liquefaction was found to have occurred in clearly defined, continuous strata, and ground motions could be reasonably well estimated.

Ground motion characteristics for the MBARI 3 case history were estimated by computing median response spectra for the site using four NGA West-2 ground motion prediction equations (GMPEs). The geometric mean of the four spectra was used as a target spectrum to which a suite of 20 motions was selected and scaled. The ground motions were selected from events with moment magnitudes within 0.5 of the Loma Prieta event ($M_w = 6.9$) and sites with source-to-site distances (R) of between approximately 15 and 30 km in order to approximate the value of $R = 21$ km at Moss Landing.

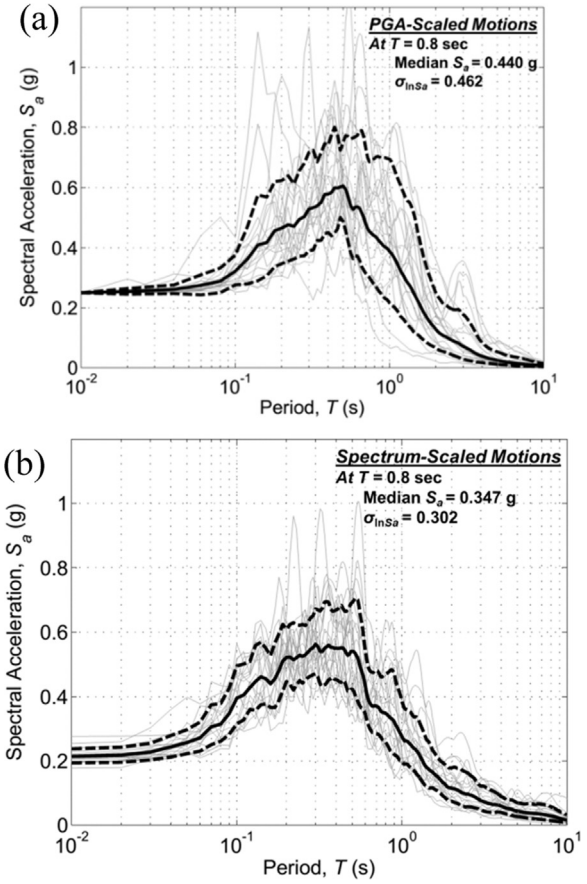

Fig. 7. Response spectra scaled: (a) to match target PGA, and (b) to match target response spectrum, for the Moss Landing MBARI 3 case history.

Fig. 7 illustrates the two sets of response spectra. Fig. 7(a) shows the 20 motions scaled to the target PGA of 0.25 g, consistent with the manner in which ground motions were developed in the OJ08 procedure. Fig. 7(b) shows spectra obtained when the motions were amplitude-scaled to minimize the least-squares arithmetic difference between the scaled motion and the target spectrum, over the broad range of periods from 0.01 to 10 s. The significant difference in spectral amplitudes shown in Fig. 7 can be traced to the fact that Olson and Johnson [18] scaled the ground motions to the value of PGA = 0.25 g used by Boulanger et al. [4] based on an estimated bedrock acceleration of 0.15 g and the application of a soft-soil site amplification factor of Idriss (1991) [12]. This is somewhat higher than the PGA of 0.21 g from the target spectrum obtained using GMPEs with appropriate V_{s30} values. Of the 39 cases analyzed by Olson and Johnson, 32 were assigned PGA values that were at least 5% higher than would be estimated using the geometric mean of the four NGA West-2 GMPEs. On average, the observed PGA values interpreted by Olson and Johnson [18] were about 35% higher than GMPE estimates, suggesting that a systematic bias toward high PGA values may exist in the OJ08 ground motions.

The differences in the two suites of ground motions influence the computed sliding block displacements shown in Fig. 8. The back-calculated yield acceleration distributions produced a median yield acceleration of 0.043 g with $\sigma_{\ln a_y} = 0.501$ for the PGA-scaled motions and a median yield acceleration of 0.035 g with $\sigma_{\ln a_y} = 0.265$ for the spectrum-scaled motions. The yield accelerations obtained using the PGA-scaled motions are considerably higher, and much more uncertain, than those obtained using the target spectrum-scaled motions. With reference to Fig. 5, stronger motions for a particular yield acceleration lead to greater displacements for that yield acceleration; as a result, a

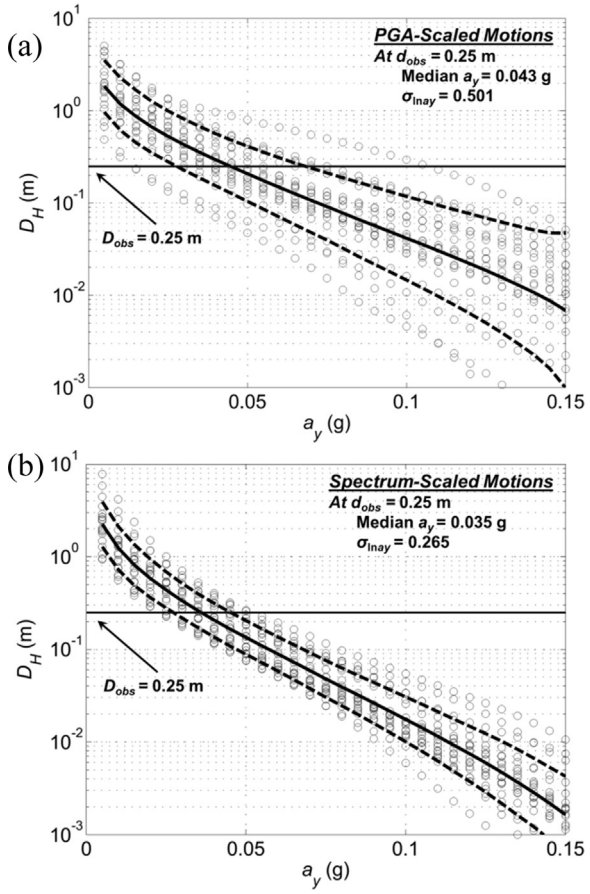

Fig. 8. Sliding block displacement vs. yield acceleration based on motions scaled: (a) to match target PGA, and (b) to match target response spectrum, for the Moss Landing MBARI 3 case history.

given observed displacement will correspond to a higher yield acceleration for a stronger suite of motions. The higher yield acceleration can be expected to lead to higher interpreted mobilized strength ratios.

3.1. Probabilistic back-calculation of mobilized residual strength ratio

In the OJ08 back-calculation procedure, the median yield acceleration was used to determine the mean residual strength of the liquefied soil. To estimate the distribution of residual strength corresponding to the observed displacement in this probabilistic analysis, the distribution of yield acceleration for a given observed displacement must be combined with the distribution of mobilized strength ratio S_r/σ'_{vo} (denoted as *MSR*) for a given yield acceleration. The distribution of *MSR* obtained this way can be expressed in the form of a cumulative distribution function (CDF), F_{MSR}:

$$F(msr|d_{obs}) = \sum_{j=1}^{n} P[MSR < msr_i|a_{y,j}]P[a_{y,j}|d_{obs}] \quad (1)$$

The first term on the right side of Eq. (1) was characterized by means of Monte Carlo pseudo-static slope stability analyses. The MBARI 3 profile was modeled as shown in Fig. 9 using SLIDE 6.0, a commercial limit equilibrium slope stability analysis program that features probabilistic functionality in which the mean and standard deviation can be defined for each input soil parameter. In these analyses, the unit weight, cohesion, and friction angle of all but the liquefied soil layer were randomized from probability distributions based on the mean and coefficient of variation (COV) values shown in Fig. 9. For the liquefied layer, the residual strength was calculated as:

$$S_{r,mob} = \sigma'_{vo} \cdot MSR \quad (2)$$

For a given horizontal seismic coefficient (a_j) and strength ratio (msr_i), a pseudo-static factor of safety was calculated using 100,000 realizations with soil properties sampled using a Latin Hypercube Sampling scheme (LHS). In addition to the familiar factor of safety (*FS*) based on the mean soil parameter values, SLIDE also reports the *probability of failure* ($P_F = P[FS < 1]$), which is the fraction of the total number samples that failed. The probability of non-exceedance of msr_i for the given a_j represents the complement of the relationship between P_F and *MSR*. A sensitivity analysis showed that the non-liquefied soil parameters had little influence on the factor of safety of the site, and thus the uncertainties in the pseudostatic analyses to characterize *MSR* resulted almost entirely from the variability in the back-calculated yield acceleration.

$$P[MSR < msr_i|a_y = a_{y,j}] = 1 - P[FS < 1|MSR = msr_i] \quad (3)$$

The probability of non-exceedance curve for *MSR* for a given yield acceleration was developed by fitting a distribution to the SLIDE data. The data obtained from the SLIDE analyses can be interpreted as a series of "success" and "failure" observations; for a given yield acceleration and *MSR*, a certain number of LHS realizations had factors of safety of either greater than 1.0 (success) or less than 1.0 (failure). This form of data observation is characterized most appropriately using binomial regression for the probability of failure on the predictor variable *MSR*. The form of the binomial mean response function depends on the assumed distribution of the errors, also known as the *link function*. For the case with *MSR* as the predictor variable, a logistic link function (in which the error term follows a logistic distribution) was found to produce the best fit to the observed data. This process was repeated for a range of horizontal seismic coefficients representing the range of yield accelerations back-calculated from the sliding block analyses (Fig. 10). Carrying through the summation of Eq. (1), CDFs of *MSR* for different yield accelerations were computed as shown in Fig. 10.

In order to obtain the CDF of the back-calculated *MSR* given the observed displacement, the probability density function (pdf) for the yield acceleration (Fig. 11a) must be combined with the CDFs for *MSR* given yield acceleration using Eq. (1). Doing so, and then differentiating $F(msr|D_{obs})$ with respect to *MSR* yields the conditional probability density function $f(msr|D_{obs})$ shown in Fig. 11(b). The median value of *MSR* for the MBARI 3 case history, based on the yield acceleration distribution computed using the *PGA*-scaled motions, was 0.122 with $\sigma_{\ln MSR} = 0.304$. Using the spectrum-scaled motions, the median *MSR* was 0.107 with $\sigma_{\ln MSR} = 0.161$. Thus, the median *MSR* values are similar (within 15% of each other), but the dispersion from the PGA-scaled motions is nearly twice as large as that from the spectrum-scaled motions.

These results do not account for uncertainty in the measured displacements upon which the entire *MSR* back-calculation process is based. Uncertainty in those observed displacements would further increase the uncertainty in back-calculated yield accelerations and *MSR* values.

3.2. Correlation of MSR values to flow failure MSR values

Olson and Johnson [18] concluded that the *MSR* values back-calculated from the lateral spreading case histories plotted consistently within the bounds of the Olson and Stark [17] *MSR* relationship derived from liquefaction flow failures, and that such strengths were applicable to sliding block analyses of lateral spreading displacements. This critically important conclusion is assessed here probabilistically, using the back-calculated lateral spread *MSR*s characterized in this section. For a given representative penetration resistance, the upper- and lower-bound *MSR*s (msr_u and msr_l) from Olson and Stark [17] were calculated using:

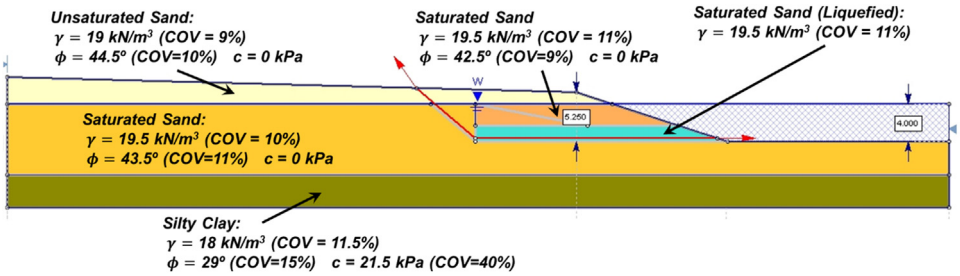

Fig. 9. Subsurface profile of the Moss Landing MBARI 3 lateral spreading site, including probabilistic input soil parameters, for use in SLIDE.

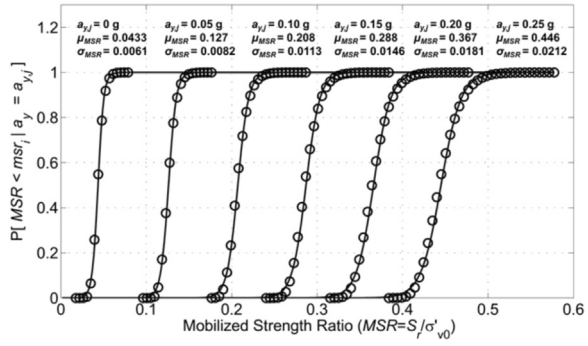

Fig. 10. Probability-of-failure data and best-fit curves for logistic mean response functions for the Moss Landing MBARI 3 case history.

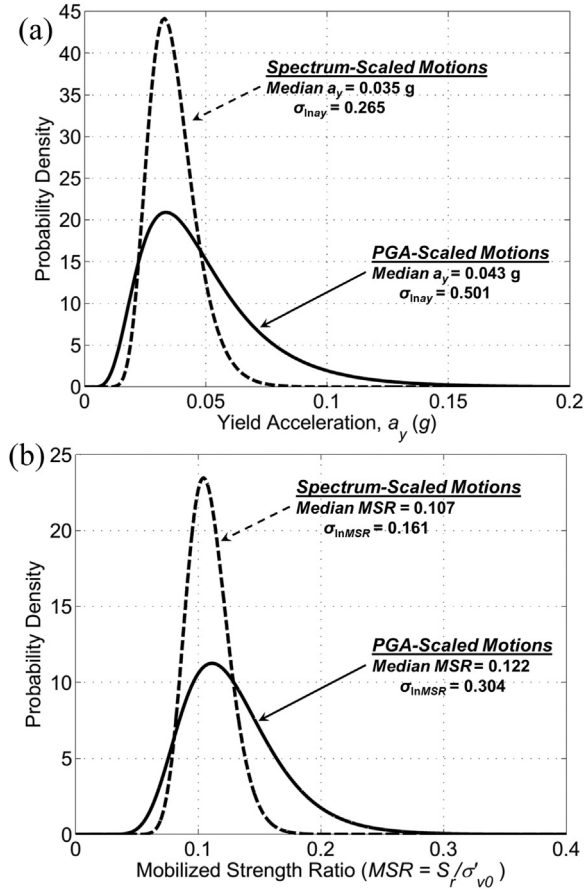

Fig. 11. Back-calculated probability density functions for: (a) yield acceleration, and (b) mobilized strength ratio for MBARI 3 case history.

$$\frac{S_r}{\sigma'_{vo}} = \begin{cases} 0.03 + 0.0143q_{c1} \pm 0.03, & q_{c1} < \sim 10 \\ 0.03 + 0.0075(N_1)_{60} \pm 0.03, & (N_1)_{60} < \sim 16 \end{cases} \quad (4)$$

For a given case history, the probability that the *MSR* estimated from the MBARI 3 case falls within the Olson and Stark bounds, denoted as $P_{MSR}(r)$, can be expressed as:

$$P_{MSR|R}(msr|r_i) = P[msr_{l,i} < MSR < msr_{u,i}|R = r_i] = P[MSR < msr_{u,i}|R = r_i] - P[MSR < msr_{l,i}|R = r_i] \quad (5)$$

The CDF of *MSR* can be used to evaluate the reasonableness of this conclusion for MBARI 3. Using q_{c1} = 10 MPa as a representative CPT resistance for the liquefied layer at MBARI 3, Eq. (4) produces lower and upper bound *MSR* values of 0.14 and 0.20, respectively. The *MSR* distribution computed here gives corresponding exceedance probabilities of 50% and 86%, so the conditional probability that the MBARI 3 *MSR* is actually within the upper and lower bounds of the Olson and Stark [17] residual strength model is 36%. However, the probability will also be influenced by uncertainty in penetration resistance, which was assumed to result from spatial variability and measurement errors. Additional uncertainty that could result from different interpretations of representative penetration resistance for individual case histories by different investigators [23] was not considered. Lognormal distributions were fit to the MBARI 3 $(N_1)_{60}$ and q_{c1} penetration test data. The probabilities of the back-calculated *MSR*s being within the Olson and Stark [17] bounds were then summed over i = 1,N_r increments of the penetration test distributions:

$$P_{MSR}(msr) = \sum_{i=1}^{N_r} P[msr_{l,i} < MSR < msr_{u,i}|R = r_i]P[R = r_i] \quad (6)$$

where N_r is the number of penetration test values in the distribution. This process indicated probabilities of *MSR* being between the upper and lower bounds of the Olson and Stark [17] mobilized strength ratio of 18% based on SPT data and 19% based on CPT data. For the *MSR* estimates derived from the spectrum-scaled motions, the same probabilities are 24% and 14% for the SPT and CPT data, respectively. The fact that the CPT-based probability is lower for the spectrum-scaled motion-derived *MSR* may seem initially surprising, given its lower uncertainty. However, this would only hold true if the median sliding block-based back-calculated *MSR*s were close to the median *MSR* from Olson and Stark's relationship. For the Moss Landing case history, this condition does not hold true for either of the back-calculated *MSR*s. The mean CPT q_{c1} of about 12 MPa would correspond to an *MSR* 0.172–0.232. The corresponding range of sliding block-based *MSR*s were considerably lower: 0.0882–0.130 for the spectrum-scaled motions, and 0.0847–0.176 for the PGA-scaled motions. Overall, these low probabilities indicate that the Olson and Stark [17] flow failure *MSR* values do not provide a strong basis for sliding block-based prediction of lateral spreading displacement for the MBARI 3 case history.

4. Probabilistic sliding block prediction of lateral spreading displacements

In order to investigate uncertainty in the displacements predicted by

the sliding block procedure, the Moss Landing MBARI 3 site was analyzed in a forward prediction framework. Particular attention was paid to characterizing the uncertainties involved in site conditions, in the mobilized strength ratio of the liquefied material, in the pseudo-static analyses used to determine the yield acceleration, and in the sliding block-based relationship between yield acceleration and permanent displacement.

4.1. Analysis procedure

For the pseudo-static analyses, the site geometry, position of the phreatic surface, position of failure surface, and parameters of the non-liquefied soils were the same as those used in the previously described back-calculation procedure (see Fig. 9). A bilinear failure surface was assumed to pass through the bottom of the liquefiable layer. Because the strength of the liquefiable material was specified as a strength ratio in this analysis, the factor of safety was found to be insensitive to the depth of the specified failure surface, but was minimized at the bottom of the liquefiable layer. The upslope limit of the failure plane was constrained such that any failure masses calculated by SLIDE had free-face ratios less than 20% to be consistent with Youd et al.'s upper limit for lateral spreads. Based on the extent of ground cracks observed by Boulanger et al. [4], which implied a free face ratio of roughly 19%, this constraint is consistent with the surface deformation patterns observed in the vicinity of MBARI 3. Without this restriction, the yield acceleration, determined from a potentially much steeper failure surface, would have been significantly lower, leading to larger predicted displacements of a sliding mass that was likely not representative of a laterally spreading mass.

To obtain statistical inputs for the strength of the liquefied material, mean and uncertainty estimates of the *MSR* were computed using the relationship of Olson and Stark [17] with their reported standard deviation, σ_{MSR} of 0.025. For a given penetration resistance value r_i, the probability of exceedance of *MSR* can be expressed via:

$$P[MSR > msr_j|R = r_i] = 1 - \Phi\left[\frac{msr_j - \mu_{msr}(r)}{\sigma_{MSR}}\right] \tag{7}$$

where Φ is the standard normal cumulative distribution function, and $\mu_{msr}(r)$ is the mean *MSR* calculated from Eq. (1).

Monte Carlo pseudostatic analyses were performed in SLIDE using Latin Hypercube Sampling, with 100,000 realizations for a series of applied horizontal seismic coefficients (a_k). In a similar manner to the back-calculation framework, the probability of failure P_F for a given horizontal acceleration a_k was determined by simply calculating the ratio of cases of $FS < 1$ to the total number of cases.

$$P[a_y < a_k|MSR = msr_j] = P[FS < 1|a_y = a_k] = \frac{N_{F,k}}{N_{tot,k}} \tag{8}$$

Similar to the back-analyses, the variation of the observed probability of failure was characterized via binomial regression, although this time with respect to the logarithm of the yield acceleration. A complementary log-log link function (where the errors are assumed to follow an extreme value distribution) was found to provide the best fit to the data. These calculations produced CDFs for the yield acceleration, with the corresponding PDFs obtained by differentiation. For the MBARI 3 site, the range of yield accelerations within one standard deviation of the median value of 0.057 was 0.036–0.13*g*.

The sliding block analyses were performed using a suite of 20 ground motions, scaled to a *PGA* of 0.25 g, to be consistent with the OJ08 procedure. The computed sliding block displacements were modeled as a mixed (discrete/continuous) random variable. In this framework, displacements below a certain threshold d_o (in this case d_o = 1 cm, after [5]) were treated as equal to $d_o/2$ (5 mm), and represented by a probability mass $P[D_H = d_o/2]$. This displacement level is considered to produce negligible physical damage. The distribution of displacements greater than 1 cm was then modeled as a truncated lognormal distribution [10], which can be expressed as:

$$P[D_H = d_i|D_H > d_0] = \begin{cases} 0 & for \quad d_i \le d_0 \\ \frac{P[D_H = d_i]}{1 - P[D_H = d_0]} & for \quad d_i > d_0 \end{cases} \tag{9}$$

For a given penetration resistance, the probability of a particular permanent displacement level can be computed by combining the probability distributions for yield acceleration, *MSR*, and permanent displacement:

$$P[D_H = d_m|R = r_i] = \sum_{j=1}^{N_q}\sum_{k=1}^{N_y} P[D_H = d_m|a_y = a_{y,k}]\times \\ \times P[a_y = a_{y,k}|MSR = msr_j]P[MSR = msr_j|R = r_i] \tag{10}$$

However, it should be recognized that penetration resistance is also uncertain. The total uncertainty of the sliding block displacement prediction can be computed by integrating (or summing) over the penetration resistance distribution, i.e., as:

$$P[D_H = d_m] = \sum_{i=1}^{N_q} P[D_H = d_m|R = r_i]P[R = r_i] \tag{11}$$

The full mixed-variable distribution for the predicted displacement can be represented by a mixed probability mass/density function (Fig. 12a) and a cumulative distribution function (Fig. 12b). These curves illustrate the discrete probability of negligible displacements (i.e., displacements below 1 cm), the probability distribution of displacements given that they are non-negligible, and the calculated probability of non-exceedance curves. By applying sliding block

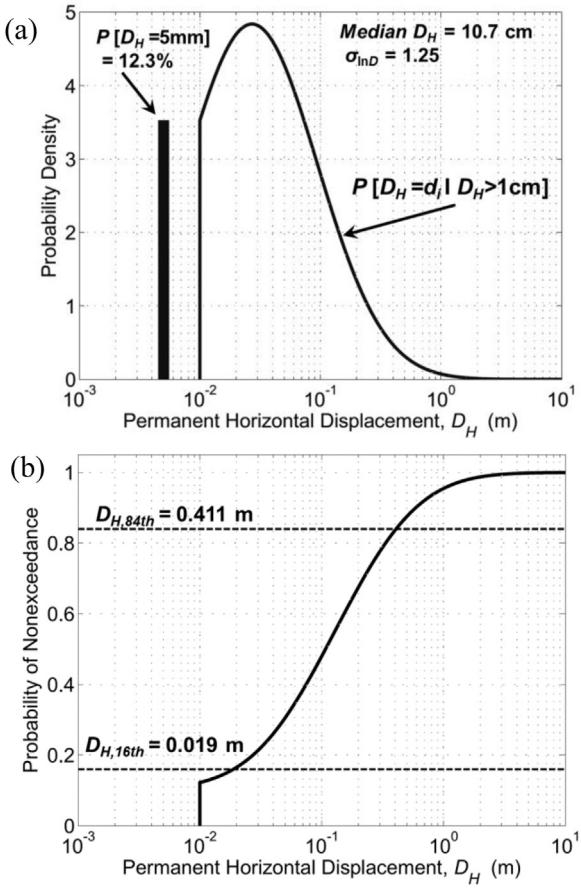

Fig. 12. Distributions of predicted displacement from sliding block and Youd et al. [25] procedures: (a) probability density functions and (b) cumulative distribution functions.

framework probabilistically, a median permanent horizontal displacement of 10.7 cm was predicted for the MBARI 3 case history, which is less than half the observed displacement of 25 cm. However, the corresponding lognormal standard deviation ($\sigma_{\ln D}$) was 1.25, which is an extraordinarily high value. For the MBARI 3 site, the estimated displacements corresponding to one standard deviation from the mean ranged from about 2 cm to approximately 41 cm. Thus, the observed displacement of 25 cm was within one standard deviation of the predicted median, mainly because of the extremely high uncertainty in the predicted displacement.

4.2. Comparison with empirical procedure

For comparison, probabilistic analyses of the lateral spreading displacements for the MBARI 3 site was carried out using the Youd et al. [25] empirical model. Uncertainty in the characterization of penetration resistances was reflected in the equivalent thickness parameter (T_{15}), which refers to the cumulative thickness of liquefiable strata with SPT resistance less than 15 blows/ft. This was characterized through a set of 1000 simulations, in which the SPT resistance of the liquefiable stratum was randomized with a median value of 20 blows/ft and $\sigma_{\ln(N1)60} = 0.749$ over 0.1 m sublayers. The SPT resistances were assumed to be spatially independent of each other. The median $(N_1)_{60}$ was based on available SPT data at the site (Mejia 1998) while the standard deviation was based on typical SPT measurement uncertainty [20]. The value of T_{15} was then determined for each realization by summing the thicknesses of the sublayers with N less than 15. A normal probability distribution for T_{15} was fitted to the simulation results; the median value of T_{15} was 1.26 m, with a standard deviation of 0.212 m. The total probability of displacement exceedance for the displacements using Youd's equation was computed by numerically integrating over the T_{15} distribution:

$$P[D_H > d_i] = \sum_{j=1}^{N} P[D_H > d_i | T_{15} = t_{15j}] P[T_{15} = t_{15,j}] \tag{12}$$

where $P[D > d_i | T_{15} = t_{15,j}]$ is lognormally distributed, with the median obtained from the Youd et al. [25] equation with $\sigma_{\ln D} = 0.464$. For the MBARI 3 case, the median predicted displacement was 0.511 m and the lognormal standard deviation was 0.496, which is only 40% of the standard deviation associated with the sliding block procedure. Comparing the two medians to the observed displacement of 0.25 m, the sliding block method under-predicts the observed displacement by a factor of 2.3, while the Youd et al. [25] method over-predicts it by a factor of about two. The differences in uncertainty can have a strong impact on lateral spreading hazard evaluation. Table 1 summarizes the percentile displacement values corresponding to the mean, plus/minus one standard deviation, and 95th percentile from both methods. The 84th and 16th percentile values differ by a factor of more than 20 using the sliding block method, compared to a factor of only 2.7 using the Youd et al. method.

A similar set of analyses performed for the Wildlife lateral spreading case history [3], where a permanent displacement of 18 cm was observed, showed median *MSR* values that were also lower than those computed by Olson and Johnson [18]. Probabilities that the *MSR* values were within the Olson and Stark [17] boundaries were 38% based on CPT data and 23% based on SPT data. In a forward analysis, the median predicted sliding block displacement was 6.8 cm with a logarithmic standard deviation, $\sigma_{\ln D} = 1.20$. For the same case, the Youd et al. [25] model predicted a median displacement of 14.1 cm with a standard deviation, $\sigma_{\ln D} = 0.464$.

Table 1
Summary of predicted permanent displacements for Moss Landing MBARI site using the Sliding Block and [25] methods.

Analysis method	Predicted displacement (m)			
	16th percentile	50th percentile	84th percentile	95th percentile
Sliding block	0.019	0.107	0.408	0.943
Youd et al. [25]	0.312	0.511	0.837	1.16

4.3. Implications for performance evaluation

Modern performance-based earthquake engineering involves the prediction of response in a probabilistic framework. Probabilistic response can be expressed in terms of two components in a PBEE framework [8] – one related to the median response and a second related to uncertainty. The second component acts as an "uncertainty amplifier" that increases the computed response for a given return period by an amount that increases with increasing uncertainty. Thus, in a PBEE framework, the uncertainty in response prediction plays a critical role in the predicted response, and consequently in predictions of physical damage and loss. Response prediction methods with low uncertainty are advantageous relative to predicting methods with high uncertainty. The sliding block procedures are notable for the extremely high uncertainty in their results. The probability distributions shown in Fig. 13 do not capture the differences in dispersion due to the differences in median values and because the linear displacement scale does not visually indicate the significant predictions of very small displacement indicated by the highly skewed sliding block distribution. Fig. 14 shows the sliding block and Youd et al. [25] distributions on a logarithmic

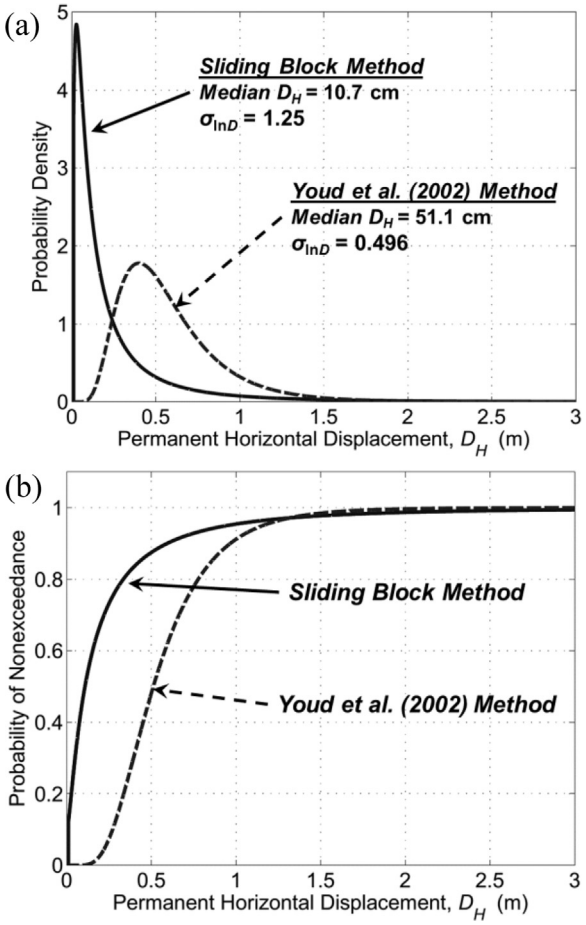

Fig. 13. Distributions of predicted displacement from sliding block and Youd et al. [25] procedures: (a) probability density functions and (b) cumulative distribution functions.

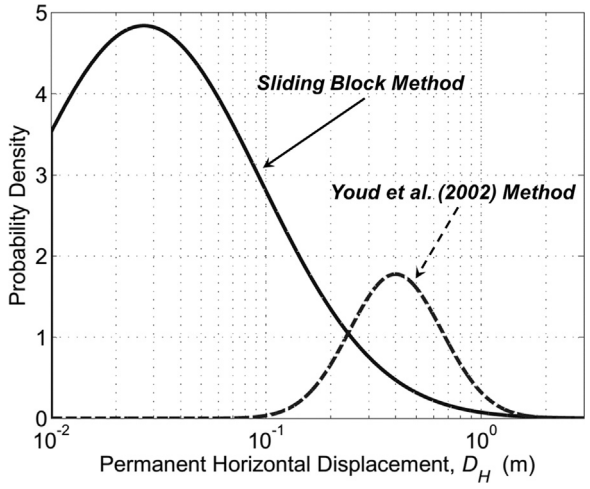

Fig. 14. Probability density functions for predicted MBARI 3 displacements using sliding block and Youd et al. [25] procedures.

scale.

5. Model uncertainty in lateral spreading analyses

A number of methodologies have been proposed for prediction of lateral spreading deformations. These methodologies are implemented in different frameworks based on laboratory test data [13,21,24], field case history data [25], and sliding block analyses [18]. Lateral spreading displacements can also be calculated from advanced numerical models, such as nonlinear finite element or finite difference analyses. Procedures based on different frameworks with different interpretations of different sets of data, however, should not be expected to produce identical, or perhaps even similar, predictions of permanent displacement. The variation of predicted results from reasonable (i.e., without known errors or biases) models represents model (or "between-model") uncertainty. The preceding portion of the paper described what can be considered to be the "within-model" uncertainties of the OJ08 and YEA02 lateral spreading displacement models. The between-model uncertainty represents the variation in lateral spreading displacements predicted by different lateral spreading models, and can be characterized by the standard deviation of the median displacements predicted by those models. Assuming independence, the total variance of the predicted lateral displacement is equal to the sum of the within- and between-model variances.

Thus far, little documented research has been performed to compare the displacements predicted by these procedures across a wide range of site and source conditions. In this section, four methods for evaluating lateral spreading are compared over a broad range of site conditions and earthquake source parameters: the empirical model developed by Youd et al. [25], hereafter referred to as YEA02, the semi-empirical model of Zhang et al. [26] based on evaluating strain potential, the Newmark-based method proposed by Olson and Johnson [18], and dynamic analyses performed using the finite-element code FLIP [9]. The computed displacements were used in an initial attempt at estimating the between-method uncertainty; standard deviations were computed as the range of computed displacements divided by a factor of 2.059 in accordance with the recommendations of Burlington and May [6] for estimation of statistical moments of small data sets.

5.1. Overview of lateral spreading methods

YEA02 is based on pure statistical regression of a large set of observed displacements against various source and site variables. Earthquake loading is characterized by the source parameters magnitude and distance, while the site parameters are the cumulative thickness (T_{15}), mean fines content (F_{15}), and mean grain size ($D50_{15}$) of liquefiable soil layers with $(N_1)_{60}$ values less than 15. Surface topography is characterized by classifying the site as a free face (*W*) or ground slope (*S*) site. The definition of the T_{15} parameter implies that displacements do not develop in materials with $N > 15$, and that, all other factors being equal, displacements are insensitive to relative density in materials with $N < 15$. This assumption is inconsistent with test data [13,21,24] that show that the development of shear strains in liquefied material varies smoothly and strongly with the initial relative density.

The ZEA04 model was developed within a semi-empirical framework based on laboratory test data. The soil profile is divided into sublayers for which the factor of safety for liquefaction (FS_{liq}) in each sublayer is evaluated using the simplified method. Laboratory-based relationships between FS_{liq} and cyclic shear strain (e.g. [13]) are then used to estimate the shear strain potential in each sublayer. The lateral displacement index (*LDI*) is calculated by integrating the estimated shear strains over the full thickness of the soil profile:

$$LDI = \int_0^{z_{max}} \gamma dz \tag{13}$$

Empirical correlations from case history data relating *LDI* and measures of ground surface topographies are used to estimate lateral displacement.

The sliding block method for predicting lateral spreading, as proposed by Olson and Johnson (OJ08), is described in detail in Section 2.4. As discussed previously, the sliding block framework assumes that the laterally spreading mass moves as a rigid body, sliding on a discrete failure plane in a rigid-perfectly plastic manner.

The finite element analysis program, FLIP, was also used to predict lateral spreading displacements for this study. FLIP uses the cocktail glass model [11] to represent the liquefiable soils. The cocktail glass model captures phase transformation behavior, and has been calibrated to produce rates of pore pressure generation and strain levels consistent with those observed in laboratory tests and implied by field observations. FLIP models the dynamic response of the soil continuum and the generation, redistribution, and eventual dissipation of excess pore pressure.

5.2. Analysis procedure

All four methods were used to predict lateral spreading displacements for a range of idealized infinite slope profiles subjected to a range of ground motions. The range of soil profiles and ground motions were selected to span the broad range of conditions in which lateral spreading displacements have been observed in the field. The ground surface inclination, thickness of the liquefiable soil, and the penetration resistance of the liquefiable material were all varied. The variable ground motion characteristics were defined in terms of source parameters, which varied according to moment magnitude and source-site distance.

5.2.1. Soil profiles

A total of 36 idealized, infinite-slope soil profiles, the basic characteristics of which are shown in Fig. 15, were defined for this study. Each profile had a total thickness of 11 m with groundwater at a depth of 2 m, and consisted of a 2 m-thick crust underlain by a layer of loose, liquefiable fill varying between 1 and 5 m in thickness. The saturated fill was a clean sand with a mean grain size of 1.75 mm. The remainder of the soil profile consisted of very dense sand that was underlain by a base of elastic bedrock. Combinations of ground slope inclination (S = {0.5°, 1.5°, 3.5°}), saturated fill thickness (T = {1, 3, 5 m}), and fill SPT resistance [$(N_1)_{60}$ = {5, 10, 15, 20 blows/ft}] were established.

5.2.2. Ground motions

To generate ground motion inputs for the FLIP and sliding block

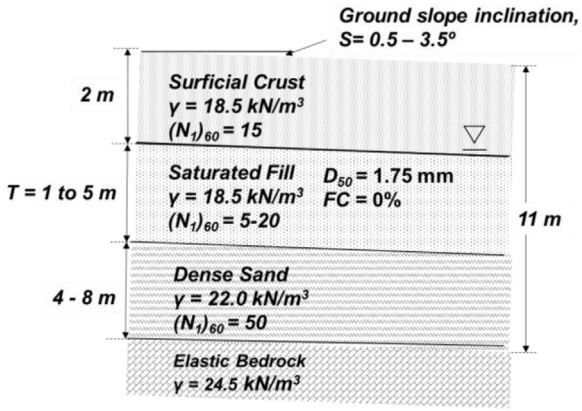

Fig. 15. Idealized subsurface profile analyzed for comparative lateral displacement study.

Table 2
Constant input GMPE parameters used to generate ground motion suites for comparative lateral spreading analysis.

Parameter	Value
Faulting Style	Strike-Slip
Shear Wave Velocity (v_{s30})	250 m/s
Dip Angle	90°
Rupture Depth	0 km (surface rupture)
Hypocentral Depth, Z_{hyp}	10.2 km
Depth to v_s = 1.0 km/s ($Z_{1.0}$)	0.48 km
Depth to v_s = 2.5 km/s ($Z_{2.5}$)	2.17 km
Rupture Width (W)	15 km

analyses, and PGA values for the strain potential analyses, target spectra were computed for a series of magnitude-distance bins as the mean of four NGA West-2 GMPEs. The magnitude-distance bins consisted of all combinations of M = {6.0, 6.5, 7.0, 7.5, 8.0} and R = {10, 20, 30, 40, 50, 70 km}. Suites of 20 ground motions for each bin were then obtained from the PEER NGAWest-2 database, and scaled using the algorithm described in Section 3.1. The target spectra were similarly estimated for each suite using the same four NGAWest-2 GMPEs. Except for M and R, all other GMPE input parameters were assumed constant with the values summarized in Table 2.

5.2.3. Implementation into lateral spreading analysis methods

The soil profiles and ground motions described above were analyzed by each lateral spreading model. In order to produce consistent predictions of median displacement between the methods, the soil parameters for all profiles were considered deterministically for this study.

5.2.3.1. Youd et al. [25]. The profiles described above were implemented into the YEA02 calculation in a relatively straightforward manner. The influence of the variable $(N_1)_{60}$ (from 5 to 20) on the predicted displacements is reflected in a stepwise manner; cases in which $(N_1)_{60} > 15$ resulted in $T_{15} = 0$, which implied zero displacement, were assigned numerical displacements of 0.5 cm for consistency with the other approaches.

5.2.3.2. Zhang et al. [26]. The ZEA04 framework requires estimation of the factor of safety of liquefaction. Using the method of Idriss and Boulanger (2008), the soil profiles were divided into 0.1 m-thick sublayers, and the cyclic resistance ratio (CRR) estimated in each sublayer using the variable N-values summarized in Section 5.2.1. The cyclic stress ratio (CSR) was computed using the median PGA and mean magnitude at the site.

5.2.3.3. Modified sliding block. A modified version of the OJ08 procedure was used in these analyses. The modifications were (a) use of motions scaled to match (in an average sense) the entire target spectrum instead of just PGA, and (b) the use of two-way sliding, which more accurately represents behavior of very flat slopes such as those considered here. Application of the OJ08 procedure to lateral spreading requires estimation of the liquefied shear strength. The value of MSR was based on the median relationship of Olson and Stark [17]. For each soil profile and $M-R$ pair, two-way sliding block analyses were performed using the 20 ground motion records for each bin and the median yield acceleration as inputs.

5.2.3.4. FLIP. FLIP analyses require the specification of a series of material parameters for each soil type, including the soil model, an indicator of liquefaction susceptibility, thickness and number of subdivisions in each stratum, density, shear wave velocity, Poisson's ratio, maximum damping parameters, $(N_1)_{60\text{-}cs}$, and friction angle. The soil profiles were divided into 1.0 m-thick sublayers. Shear wave velocities were correlated to SPT resistance and vertical effective stress using an empirical relationship for Holocene sands [22]. Friction angle was correlated to SPT resistance and vertical effective stress [14]. The displacements predicted using FLIP were processed using the same method used for the OJ08 method.

5.3. Results of analyses

The combinations of the three ground slopes, three liquefiable layer thicknesses, four SPT resistances, five moment magnitudes, six source-to-site distances, and 20 ground motions produced too much data to show in its entirety.

Fig. 16 shows the computed displacements for all combinations of SPT resistance, liquefiable layer thickness, and earthquake magnitude for 1.5% slopes located 20 km from the ground motion source. Combinations of parameters that produced very small displacements, i.e., less than 1 cm, were treated in a manner similar to that previously described for the OJ08 case – displacements less than 1 cm were assigned values of 0.5 cm. The first, and most obvious, observation is that the procedures produce very different median estimates of permanent displacement. It is also apparent that the computed displacements increase with increasing magnitude and decrease with increasing SPT resistance. The displacements computed by the YEA02 and ZEA04 methods increase significantly with increasing liquefiable layer thickness, but the sliding block and FLIP methods are insensitive to liquefiable layer thickness. The displacements predicted by the FLIP analyses can be seen to be consistently higher than those predicted by the empirical procedures, particularly for the case of a relatively thin (1 m) liquefiable layer and for the higher soil densities. For thicker profiles, the YEA02 and ZEA04 procedures predict larger displacements that are more consistent with the FLIP predictions. The YEA02 procedure predicts negligible displacement for the $(N_1)_{60} = 20$ case. Finally, the values predicted by OJ08 were consistently the lowest of the four procedures, and appeared to be closest to the other approaches for the loosest soil conditions.

The logarithmic standard deviations of the median lateral spreading displacements are presented for all combinations of SPT resistance, liquefiable layer thickness, ground slope, and earthquake magnitude for slopes located 20 km from the ground motion source in Fig. 17. Some combinations of these parameters produced very small displacements; standard deviation values are not presented for cases in which two or more procedures predicted median displacements less than 1 cm. The between-model dispersion can be seen to be extremely high with $\sigma_{\ln D}$ values generally greater than 1.0. The dispersion tends to decrease with increasing magnitude for looser soils and increase with increasing magnitude for denser soils; the dispersion at $(N_1)_{60} = 20$, however, is affected by the negligible displacement values automatically produced by the T_{15} definition used in YEA02. The dispersion for larger magnitude earthquakes (M ≥ 7) generally decreases with increasing ground

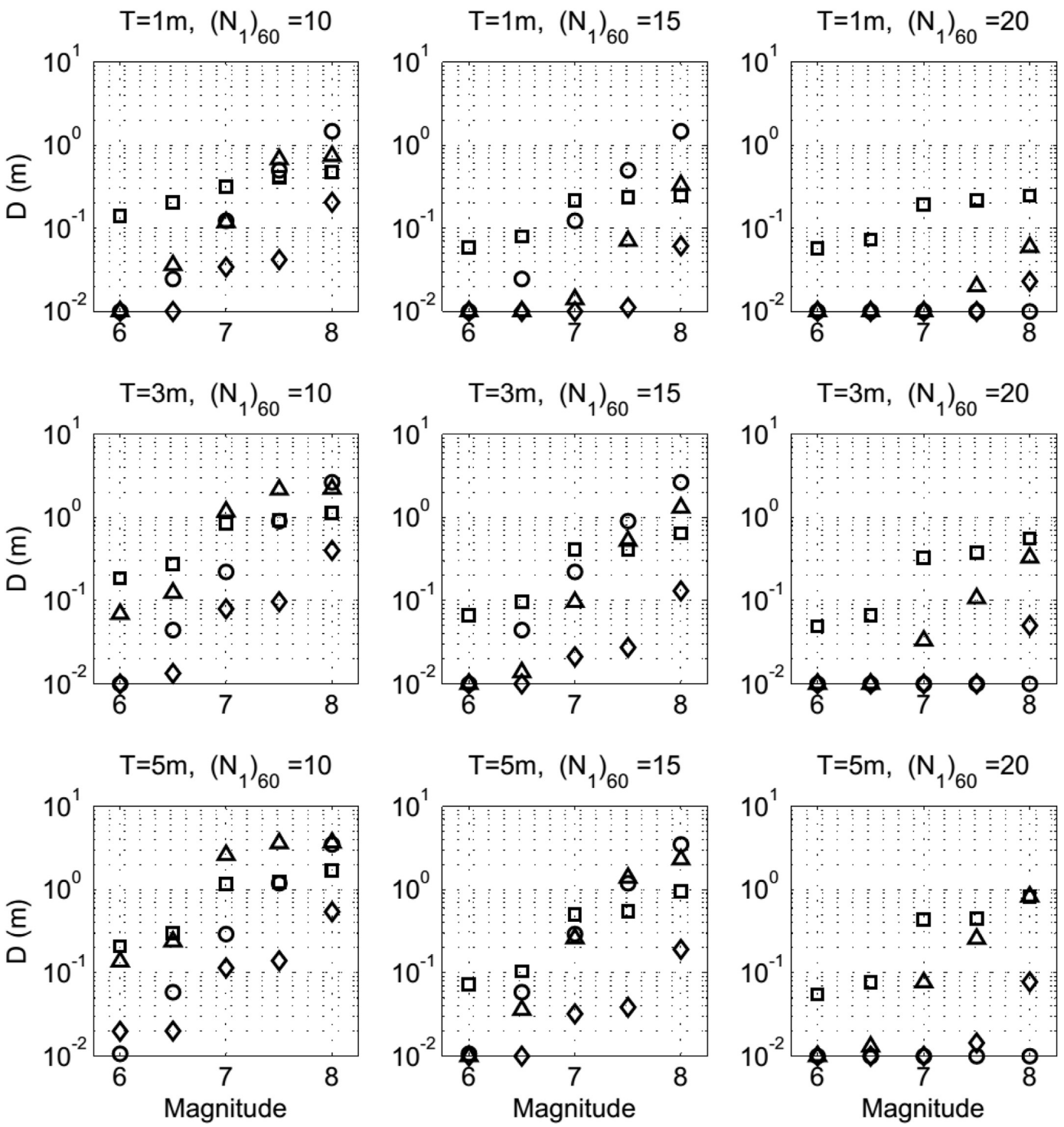

Fig. 16. Summary of median predicted displacements versus moment magnitude, for lateral spreading analysis cases where $(N_1)_{60}$ = 10, 15, and 20, and S = 1.5°.

slope but increases with increasing ground slope for all magnitudes when $(N_1)_{60}$ = 20.

5.4. Implications

The comparative analyses show, for the range of profiles and ground motions used in this investigation, an extremely high level of between-model dispersion. The agreement between the four models is poor, leading to between-model dispersions on the order of 1.0–2.0. If the sliding block method is removed from the comparisons, the between-model dispersions are significantly reduced, with dispersions generally between 0.5 and 1.0 for SPT resistances of 10 and 15 and higher magnitudes. While these values are lower, they are still quite high, particularly for $M < 7$, and illustrate the profession's current challenges in predicting lateral spreading displacement.

6. Summary and conclusions

Sliding block analyses have been widely used for evaluation of seismic slope stability hazards for the past 40 years. The fundamental

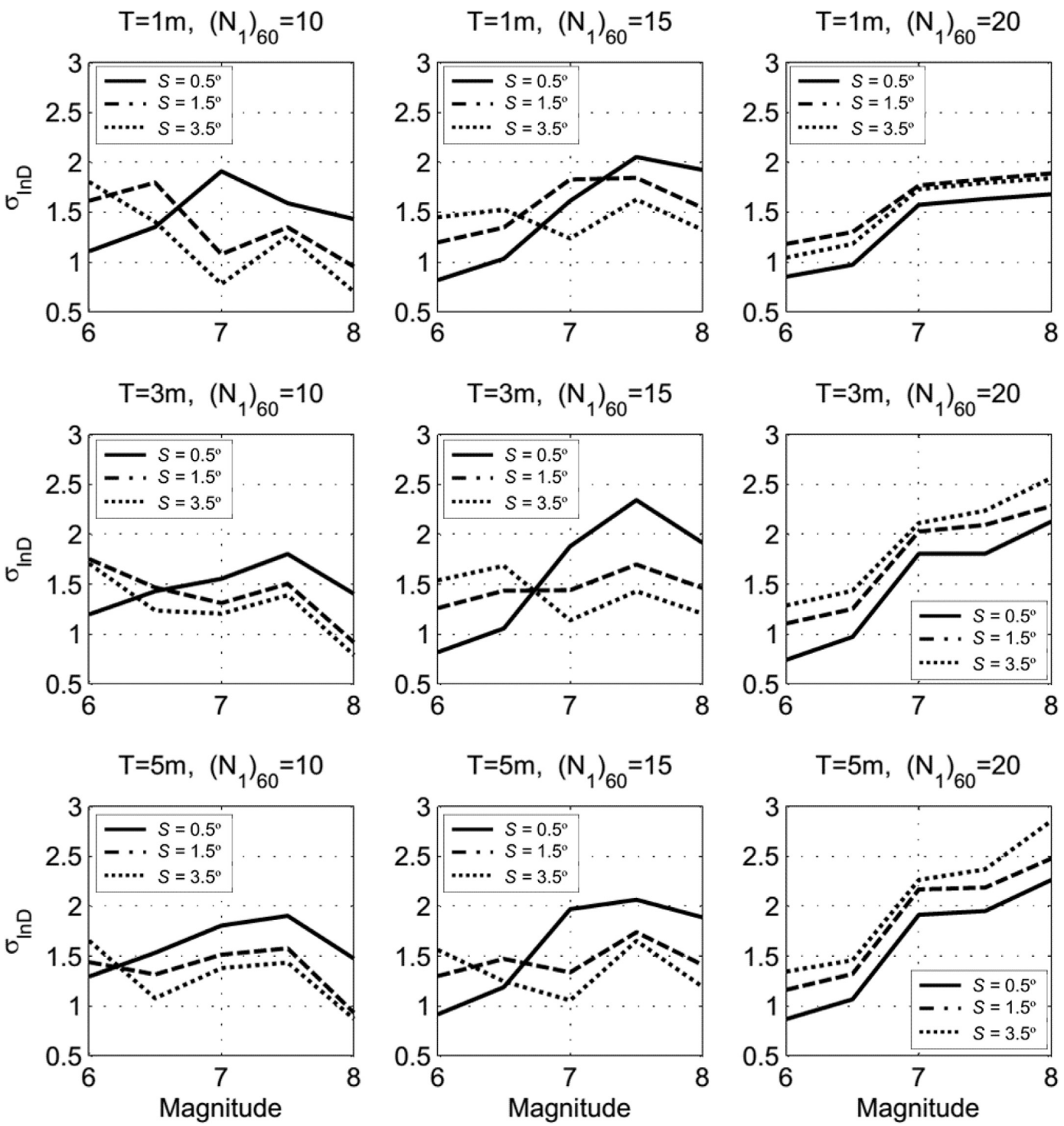

Fig. 17. Summary of within-model standard deviations versus moment magnitude, for lateral spreading analysis cases where $(N_1)_{60}$ = 10, 15, and 20.

assumptions of the sliding block approach – that a rigid mass of soil slides on a thin failure surface upon which shearing resistance remains constant – are approximately satisfied for many important, practical cases. Lateral spreads, however, typically involve distributed straining of materials whose shearing resistance fluctuates over the course of ground shaking, which is inconsistent with the assumptions of sliding block analyses. These inconsistencies motivated an investigation of the applicability of sliding block analyses to lateral spreading problems.

The implementation of the widely-used sliding block procedure of Olson and Johnson [18] is based on the back-calculation of apparent shearing resistance from a series of lateral spreading case histories. The observed permanent displacements were used in sliding block analyses to estimate yield acceleration values that were consistent with the observed displacements. The yield accelerations were then used in pseudo-static stability analyses to estimate the apparent shearing resistances of the soils considered to have liquefied in the lateral spreading events. Those apparent shearing resistances were then found to be consistent with shearing resistances, i.e., residual strengths, obtained from flow slide case histories.

The development of any semi-empirical procedure is strongly influenced by the (case history) data upon which it is based, and on the information available with which to interpret the mechanism(s) of

deformation involved in the case histories. The characteristics of the lateral spreading database used to develop the sliding block lateral spreading procedure were examined. A probabilistic analysis of the back-calculation procedure was conducted with particular attention paid to the manner in which the ground motions used in the sliding block yield acceleration calculations were developed. These analyses allowed estimation of the probability distribution of apparent shearing resistance, which then allowed examination of the extent to which the apparent shearing resistances back-calculated from lateral spreads were consistent with residual strengths back-calculated from liquefaction flow failures. Finally, the distribution of apparent shearing resistance was used in probabilistic sliding block analyses to evaluate the probability distribution of computed displacements.

The complexity of lateral spreading and the limited number of well-documented lateral spreading case histories have led to a number of different approaches to estimation of lateral spreading displacement. The different approaches are generally known to produce different levels of estimated displacement when applied to the same problem. A systematic comparison of computed lateral spreading displacements was undertaken considering a broad range of site conditions and ground motions.

The mechanisms involved in lateral spreading are complex and influenced by factors that are difficult to characterize in advance of an earthquake. As a result, prediction of lateral spreading displacements is quite challenging and the best approach to making those predictions is not clear at this time. The development of multiple approaches based on different types of data and different types of analyses is therefore natural and appropriate. As more data becomes available, one or more prevailing approaches are likely to emerge. Until that time, however, it is important to understand the benefits and limitations of the approaches currently in use. The research described in this paper has led to several conclusions:

1. The existing case history database is limited in terms of the number of case histories and their distribution over various predictive variables known to influence lateral spreading deformations. Very few case histories have been investigated sufficiently to provide the level of subsurface data needed to performed detailed analyses.
2. The case history database used to develop the most commonly used sliding block procedure is smaller but broader and more uniform with respect to several important predictive variables than previous databases. It is, however, heavily weighted toward steeper slopes than are typically involved in lateral spreads in the field. A significant portion of the database is comprised of slopes so steep that mechanisms other than lateral spreading are likely to have contributed to the observed displacements.
3. Back-calculations based on dynamic analyses are sensitive to the characteristics of the ground motions used as inputs to those analyses. The back-calculation procedure used to develop the sliding block lateral spreading procedure used measured or estimated peak ground acceleration values of unknown uncertainty, typically obtained from reports of the investigations of the individual case histories. The availability of more recent ground motion prediction equations, and particularly the use of event terms for the causative earthquakes, would likely lead to improved estimates of peak ground acceleration for many of the case histories.
4. The back-calculation procedure used to develop the sliding block procedure scaled suites of 20 motions to the measured/estimated peak ground acceleration values. Such scaling typically provides good representation of the high-frequency ground motion amplitudes, but highly variable intermediate and, particularly, low-frequency amplitudes. The response of a liquefied site, particularly the post-triggering response of the softened soil, is sensitive to a broad range of frequencies, so consideration of spectral shape is important. Scaling solely to peak ground acceleration can lead to bias, and surely leads to increased uncertainty, in the computed response.
5. Probabilistic evaluation of the back-calculated yield acceleration for the well-documented Monterey Bay Aquarium Research Institute case history showed that the median back-calculated yield acceleration was 23% higher with peak acceleration-scaled motions than with spectrum-scaled motions and the (logarithmic) standard deviation of yield acceleration was 89% higher. This illustrates a significant source of bias in the procedure.
6. Probabilistic evaluation of the apparent shearing resistance, expressed in terms of a mobilized strength ratio, showed that the median ratio and (logarithmic) standard deviation were respectively 14% and 89% higher for the peak acceleration-scaled motions than for the spectrum-scaled motions. Further analyses showed that the probability of the back-calculated mobilized strength ratios being within the upper and lower bounds of the flow slide-based strength ratios for this case history was less than 25% for either set of motions.
7. Probabilistic forward predictions of lateral spreading displacements allowed evaluation of probability distributions of computed displacements. For the Monterey Bay Aquarium case, the predicted median displacement of 10.7 cm was lower than the observed displacement of 25 cm, and the (logarithmic) standard deviation of displacement was 1.25. A similar analysis of the Wildlife Liquefaction Array lateral spreading case history resulted in a median predicted displacement of 6.8 cm, which was lower than the observed 18 cm displacement, and a (logarithmic) standard deviation of 1.20. Thus, the median sliding block displacements were significantly lower than the observed values and the uncertainties in the predicted values were extraordinarily large for both case histories.
8. A great deal of dispersion exists between the currently available methods for predicting lateral spreading displacements. Simplified methods such as the sliding block, empirical, and strain potential models generally tend to predict significantly lower displacements than those predicted by advanced numerical methods, particularly in cases with thin liquefiable layers and lower levels of ground shaking. For cases with thicker liquefiable layers and larger ground motion amplitudes and durations, the empirical and strain potential methods showed better agreement with numerical models. Across a wide range of conditions, displacements predicted by the sliding block method were consistently lower than those predicted by the other three methods, and significantly lower than those predicted using numerical methods.

References

[1] Bartlett SF, Youd TL. Empirical prediction of liquefaction-induced lateral spread. J Geotech Eng 1992;121(4):316–29.
[2] Baziar MH, Dobry R, Elgamal A-WM. Engineering evaluation of permanent ground deformations due to seismically induced liquefaction. Technical Rep. No. NCEER-92-0007, National Center for Earthquake Engineering Research,State Univ. of New York at Buffalo, Buffalo, N.Y.
[3] Bennett MJ, McLaughlin PV, Sarmiento JS, Youd TL. Geotechnical investigation of liquefaction sites, Imperial Valley, California. USGS Open-File Rep. No. 1984. 84-252, Washington, D.C.
[4] Boulanger RW, Mejia LH, Idriss IM. Liquefaction at moss landing during Loma Prieta earthquake. J Geotech Geoenviron Eng 1997;123(5):453–67.
[5] Bray JD, Travasarou T. " Simplified procedure for estimating earthquake-induced deviatoric slope displacements.". J Geotech Geoenviron Eng 2007;133(4):381–92.
[6] Burlington RS, May Jr. DC. Handbook of probability and statistics. New York: McGraw-Hill; 1970.
[7] Castro G. On the behavior of soils during earthquakes–liquefaction. Dev. Geotech. Eng. 1987;42:169–204.
[8] Cornell CA, Jalayer F, Hamburger RO, Foutch DA. Probabilistic basis for 2000 SAC federal emergency management agency steel moment frame guidelines. J Struct Eng 2002;128(4):526–33.
[9] FLIP Consortium. FLIP (ver. 7.2.3). August 2011.
[10] Greene WH. Econometric analysis. International edition. New Jersey: Prentice Hall; 2003.
[11] Iai S, Tobita T, Ozutsumi O, Ueda K. Dilatancy of granular materials in a strain space multiple mechanism model. Int J Numer Anal Methods Geomech 2011;35(3):360–92.
[12] Idriss IM. Response of soft soil sites during earthquakes. Duncan JM, editor. Proc.,

H. Bolton Seed Memorial Symp. 2. Vancouver, B.C., Canada: BiTech Publishers Ltd.; 1991. p. 273–89.
[13] Ishihara K, Yoshimine M. Evaluation of settlements in sand deposits following liquefaction during earthquakes. Soils Found. 1992;32(1):173–88.
[14] Kulhawy FH, Mayne PW (1990). *Manual on estimating soil properties for foundation design* (No. EPRI-EL-6800). Electric Power Research Inst., Palo Alto, CA (USA); Cornell Univ., Ithaca, NY (USA). Geotechnical Engineering Group.
[15] Moss RE, Hollenback JC. Discussion of 'analyzing liquefaction-induced lateral spreads using strength ratios' by SM Olson and CI Johnson. J Geotech Geoenviron Eng 2009;135(12):2006–8.
[16] Newmark NM. Effects of earthquakes on dams and embankments. Geotechnique 1965;15(2):139–60.
[17] Olson SM, Stark TD. Liquefied strength ratio from liquefaction flow failure case histories. Can Geotech J 2002;39(3):629–47.
[18] Olson SM, Johnson CI. Analyzing liquefaction-induced lateral spreads using strength ratios. J Geotech Geoenviron Eng 2008;134(8):1035–49.
[19] Park D, Kutter BL. Discussion of analyzing liquefaction-induced lateral spreads using strength Ratios by SM Olson and CI Johnson. J Geotech Geoenviron Eng 2009;135(12):2008–10.
[20] Phoon KK, Kulhawy FH. Characterization of geotechnical variability. Can Geotech J 1999;36(4):612–24.
[21] Tokimatsu K, Asaka Y. Effects of liquefaction-induced ground displacements on pile performance in the 1995 Hyogoken-Nambu earthquake. Soils Found. 1998;2:163–77 Special Issue.
[22] Wair BR, DeJong JT, Shantz T. Guidelines for estimation of shear wave velocity profiles. Berkeley, California: Pacific Earthquake Engineering Research Center; 2012.
[23] Wride CE, McRoberts EC, Robertson PK. Reconsideration of case histories for estimating undrained shear strength in sandy soils. Can Geotech J 1999;36(5):907–33.
[24] Wu J (2002). Liquefaction Triggering and Post-Liquefaction Deformation of Monterey 0/30 Sand Under Uni-Directional Cyclic Simple Shear Loading. Ph.D. Thesis, University of California, Berkeley.
[25] Youd TL, Hansen CM, Bartlett SF. Revised multilinear regression equations for prediction of lateral spread displacement. J Geotech Geoenviron Eng 2002;128(12):1007–17.
[26] Zhang G, Robertson PK, Brachman RWI. Estimating liquefaction-induced lateral displacements using the standard penetration test or cone penetration test. J Geotech Geoenviron Eng 2004;130(8):861–71.